

Jet Discrimination with Quantum Complete Graph Neural Network

Yi-An Chen* and Kai-Feng Chen

Department of Physics, National Taiwan University, Taipei, Taiwan

(Dated: March 11, 2024)

Machine learning, particularly deep neural networks, has been widely utilized in high energy physics and has shown remarkable results in various applications. Moreover, the concept of machine learning has been extended to quantum computers, giving rise to a new research area known as quantum machine learning. In this paper, we propose a novel variational quantum circuit model, **Quantum Complete Graph Neural Network** (QCGNN), designed for learning complete graphs. We argue that QCGNN has a polynomial speedup against its classical counterpart, due to the property of quantum parallelism. In this paper, we study the application of QCGNN through the challenging jet discrimination, where the jets are represented with complete graphs. Subsequently, we conduct a comparative analysis with classical graph neural networks to establish a benchmark.

I. INTRODUCTION

The proton-proton collision events in the Large Hadron Collider (LHC) produce jets from hard scattering events. Jets are collimated sprays of particles, formed through the hadronization of elementary particles. Jet discrimination, i.e., identifying the type of elementary particle that initiates the jet, is one of the challenging tasks in particle physics.

Deep neural networks (DNNs), celebrated for their architectural flexibility and intricate expressiveness, has been widely adopted in various applications, including high energy physics (HEP) [1–13]. The design for a DNN model tailored for jet discrimination presents a significant challenge due to the indeterminate number of constituent particles within jets. Several data representations for jets and DNN models have been proposed. These include techniques such as concatenating particle information into two-dimensional images (usually the pseudorapidity η versus the azimuthal angle ϕ) [4–7], or sorting particles in a specific way (e.g. by transverse momentum) [7–9]. Despite the simplicity of these data representations, the former loses information regarding individual particles and translational invariance, while the latter disregards permutation invariance. To retain both the information of each individual constituent particles and the symmetries, the utilization of graph representations of jets, along with graph neural networks (GNNs), has been increasingly employed in recent research [10–15].

In the upcoming high luminosity LHC (HL-LHC), the data is expected to be increased by several orders of magnitude in comparison to the LHC. Hence, efficient methodologies and novel technologies in data analysis are demanded. Quantum machine learning (QML) [16–20], namely implementing machine learning with quantum computers, may be one of the candidates. QML is expected to learn differently by leveraging the unique properties of quantum systems, such as superposition and

entanglement, which cannot be efficiently simulated using classical computers. QML has also been studied on several HEP applications [21], e.g., particle track reconstruction [22], events classification [23, 24], jet discrimination [25].

In this paper, we introduce the **”Quantum Complete Graph Neural Network (QCGNN)”,** a variational quantum circuit model [26–28] specifically designed for learning complete graphs [29], showcasing a polynomial speedup over its classical counterparts by utilizing the property of quantum parallelism. The application of QCGNN is studied through jet discrimination of two-prong jets ($H \rightarrow b\bar{b}$) and three-prong jets (fully hadronic top jets) against light quark (u, d, c, s) jets, where we represent jets using complete graphs.

The main structure of this paper is as follows. In section II, prerequisites and the detail of QCGNN are given, and we also discuss the computational speedup comparing to its classical counterpart. Section III contains the experimental setup for jet discrimination, and the results will be shown in section IV. Finally, we summarize this paper in the final section V.

II. METHODOLOGY

A. Graph Neural Network

Graphs are ubiquitous data structures that represent relationships and connections between entities. Analyzing and extracting valuable information from these graph-structured data is a fundamental challenge in modern data science and machine learning. To address this challenge, GNN has emerged as a powerful and versatile framework for learning from graph-structured data, e.g., social recommendation [30], biology [31], chemistry [32], etc.

A graph G is described by its set of nodes V and edges E , denoted as $G = (V, E)$. Let N be the number of nodes, and E_{ij} the edge from node V_i to node V_j . Throughout this paper, the graphs are assumed to be *undirected* ($E_{ij} = E_{ji}$) and *unweighted* (all edges have equal weights). Furthermore, a graph is said to be *com-*

* r08222011@gmail.com

plete [29] if all pairs of nodes are connected. For each node V_i , there is a corresponding feature vector $\mathbf{x}_i \in \mathbb{R}^D$, where D is the dimension of the features.

Graphs are permutation invariant, namely changing the indices of nodes does not change the information of the graph. The basic idea of GNN is to design a neural network that satisfies the property of permutation invariance. In this paper, we consider message passing GNNs (MPGNNs) [33], which can be described by ¹

$$\mathbf{x}_i^{(k)} = \gamma^{(k)} \left(\mathbf{x}_i^{(k-1)}, \bigoplus_{\substack{j \in V \\ E_{ij} \neq 0}} \Phi^{(k)}(\mathbf{x}_i^{(k-1)}, \mathbf{x}_j^{(k-1)}) \right) \quad (1)$$

where $\Phi^{(k)}$ extracts the information between nodes, and $\gamma^{(k)}$ updates the node features in the k -th iteration. To satisfy the property of permutation invariance, the aggregation function \bigoplus is the crucial part for GNNs, such as **SUM**, **MEAN**, **MAX**, **MIN**, etc.

B. Quantum Complete Graph Neural Network

In the noisy intermediate-scale quantum (NISQ) era [34] of quantum computers, the variational quantum circuit (VQC) [26–28] is one of the intuitive ways to realize quantum neural networks. Typically, a VQC can be formulated as

$$f(\mathbf{x}; \boldsymbol{\theta}) = \langle 0 | U^\dagger(\mathbf{x}; \boldsymbol{\theta}) P U(\mathbf{x}; \boldsymbol{\theta}) | 0 \rangle$$

for some Pauli string observable P and unitary matrix U . The unitary matrix encodes the data \mathbf{x} to the quantum state and contains several tunable parameters $\boldsymbol{\theta}$. The parameters can be updated through gradient descent [35–38] with an appropriate loss function. Usually, the unitary matrix U can be split into encoding part and parametrized part, denoted as U_{ENC} and U_{PARAM} correspondingly.

The QCGNN consists of two qubit registers: an index register (IR) and a neural network register (NR), with n_I and n_Q qubits respectively. Consider a complete graph (*undirected* and *unweighted*), we set $n_I = \lceil \log_2(N) \rceil$, where N is the number of nodes. The quantum state in IR will be initialized to n_I uniform basis, namely

$$|\psi_0\rangle = \frac{1}{\sqrt{N}} \sum_{i=0}^{N-1} |i\rangle |0\rangle^{\otimes n_Q}, \quad (2)$$

where $|0\rangle^{\otimes n_Q}$ is the initial quantum state in NR. The node feature \mathbf{x}_i will be encoded through some unitary

matrix $U_{\text{ENC}}(\mathbf{x}_i)$, controlled by the corresponding controlled basis in IR with controlled values being the binary representation of i , denoted as $C_{\text{bin}(i)} U_{\text{ENC}}(\mathbf{x}_i)$, i.e.,

$$C_{\text{bin}(i)} U_{\text{ENC}}(\mathbf{x}_i) (|j\rangle |0\rangle^{\otimes n_Q}) = \delta_{ij} |j\rangle U_{\text{ENC}}(\mathbf{x}_i) |0\rangle^{\otimes n_Q}$$

Subsequently, some parametrized unitary matrix $U_{\text{PARAM}}(\boldsymbol{\theta})$ will be applied to NR. The quantum state is then evolved to

$$\begin{aligned} |\psi\rangle &= \frac{1}{\sqrt{N}} U_{\text{PARAM}}(\boldsymbol{\theta}) \bigotimes_{i=0}^{N-1} C_{\text{bin}(i)} U_{\text{ENC}}(\mathbf{x}_i) |\psi_0\rangle \\ &= \frac{1}{\sqrt{N}} \sum_{i=0}^{N-1} |i\rangle U_{\text{PARAM}}(\boldsymbol{\theta}) U_{\text{ENC}}(\mathbf{x}_i) |0\rangle^{\otimes n_Q}. \end{aligned}$$

Consider a Pauli string observable P applied on NR. The expectation value of the measurement is

$$\begin{aligned} \langle \psi | P | \psi \rangle &= \frac{1}{N} \sum_{i=0}^{N-1} \langle 0 |^{\otimes n_Q} U_{\text{ENC}}^\dagger(\mathbf{x}_i) U_{\text{PARAM}}^\dagger(\boldsymbol{\theta}) \\ &\quad P U_{\text{PARAM}}(\boldsymbol{\theta}) U_{\text{ENC}}(\mathbf{x}_i) |0\rangle^{\otimes n_Q}, \end{aligned}$$

which is just the self-correlations of each node. To get the correlations with other nodes, we consider a $2^{n_I} \times 2^{n_I}$ Hermitian matrix J full of ones as an observable of IR. Observing that

$$\begin{aligned} \langle \psi | J \otimes P | \psi \rangle &= \frac{1}{N} \sum_{i=0}^{N-1} \sum_{j=0}^{N-1} \langle 0 |^{\otimes n_Q} U_{\text{ENC}}^\dagger(\mathbf{x}_j) U_{\text{PARAM}}^\dagger(\boldsymbol{\theta}) \\ &\quad P U_{\text{PARAM}}(\boldsymbol{\theta}) U_{\text{ENC}}(\mathbf{x}_i) |0\rangle^{\otimes n_Q}. \end{aligned} \quad (3)$$

Notice that Eq.(3) calculates all the correlations over pairs (including self-correlations), or to be more precise, the average of the correlations. Define the correlation function $k(\mathbf{x}_i, \mathbf{x}_j; P)$ as

$$\begin{aligned} k(\mathbf{x}_i, \mathbf{x}_j; P) &= \langle 0 |^{\otimes n_Q} U_{\text{ENC}}^\dagger(\mathbf{x}_j) U_{\text{PARAM}}^\dagger(\boldsymbol{\theta}) \\ &\quad P U_{\text{PARAM}}(\boldsymbol{\theta}) U_{\text{ENC}}(\mathbf{x}_i) |0\rangle^{\otimes n_Q} + h.c. \end{aligned} \quad (4)$$

The correlation function $k(\mathbf{x}_i, \mathbf{x}_j; P)$ is also symmetric, i.e., $k(\mathbf{x}_i, \mathbf{x}_j; P) = k(\mathbf{x}_j, \mathbf{x}_i; P)$. Practically, the matrix J can be decomposed as

$$J = \bigotimes_{q=0}^{n_I-1} \begin{bmatrix} 1 & 1 \\ 1 & 1 \end{bmatrix} = \bigotimes_{q=0}^{n_I-1} (I_q^{\text{IR}} + X_q^{\text{IR}}), \quad (5)$$

where X_q^{IR} refers to the Pauli-X observable of the q -th qubit in IR, and I_q^{IR} is the identity matrix. The expansion of Eq.(5) has $2^{n_I} \approx N$ different combinations of Pauli string observables. By summing over the expectation values of all combinations in Eq.(5), we get the average of correlation functions of all pairs, corresponding

¹ The formula is followed from pytorch-geometric documentation https://pytorch-geometric.readthedocs.io/en/latest/tutorial/create_gnn.html

to **MEAN** in classical GNN’s aggregation function. One could also remove self-correlations by simply considering

$$J \rightarrow J - \bigotimes_{q=0}^{N-1} I_q^{\text{IR}}. \quad (6)$$

Assuming that the computational cost for **calculating the correlation between a pair of nodes** is approximately the same order in both classical and quantum models, we further presume that the additional cost for decomposing multi-controlled gates can be neglected when compared to the deep parametrized gates $U_{\text{PARAM}}(\theta)$. With these assumptions, QCGNN requires $2^{n_I} \approx O(N)$ operations to calculate the average correlation functions between all pairs, while for its classical counterpart, we need $O(N^2)$ operations.

QCGNN can also be extended to *weighted* graphs. In extremely simple cases, consider an *undirected* and *weighted* graph, for which its adjacency matrix A can be expressed as the outer product of a vector $|w\rangle = \sum_i w_i |i\rangle$, where the edge weight $A_{ij} = w_i w_j$. Instead of initializing IR uniformly, we initialize the quantum state as

$$\sum_{i=0}^{N-1} \frac{1}{\sqrt{N}} |i\rangle |0\rangle^{\otimes n_Q} \rightarrow \sum_{i=0}^{N-1} \frac{w_i}{\sqrt{\langle w|w\rangle}} |i\rangle |0\rangle^{\otimes n_Q},$$

such that when calculating terms in Eq.(3), we have

$$\frac{1}{N} k(\mathbf{x}_i, \mathbf{x}_j; P) \rightarrow \frac{w_i w_j}{\langle w|w\rangle} k(\mathbf{x}_i, \mathbf{x}_j; P) = \frac{A_{ij}}{\text{Tr}(A)} k(\mathbf{x}_i, \mathbf{x}_j; P).$$

The vector $|w\rangle$ can be encoded through **AMPLITUDE EMBEDDING**². To generalize to *directed* and *weighted* graphs, we observe that any matrix can be decomposed into symmetric and skew-symmetric matrices. Since both matrices are normal, they are diagonalizable according to the spectral theorem. One can repeat the method above for each eigenbasis individually and multiply by a factor proportional to the corresponding eigenvalue. However, the additional computation cost from diagonalizing matrices and **AMPLITUDE EMBEDDING** might overshadow the speedup advantage. For practical usage, we only consider the application of QCGNN to *undirected* and *unweighted* graphs.

III. EXPERIMENTAL SETUP

A. Dataset For Jet Discrimination

The Monte Carlo simulations used in jet discrimination are generated with $\sqrt{s} = 13$ TeV using MADGRAPH5

[39], PYTHIA8 [40] and DELPHES [41, 42] for simulation of hard scattering process, QCD hadronization and detector responses respectively. Jets are clustered by the anti- k_T algorithm [43] with $R = 0.8$, and implemented with FASTJET [44]. The 2-prong jets ($Z' \rightarrow ZH, H \rightarrow b\bar{b}$) and the 3-prong jets ($Z' \rightarrow t\bar{t}, t \rightarrow bW^+, \bar{t} \rightarrow \bar{b}W^-$) are produced from the decay of the hypothetical vector bosons [45], while the background 1-prong QCD jets are produced with light quarks ($q = u, d, c, s$).

In this paper, we represent each jet through a complete graph. Each node corresponds to a particle in the jet, and the node features are related to the energy flow information, including the transverse momentum fraction $z_i = p_{Ti}/p_{Tjet}$, the relative pseudorapidity $\Delta\eta_i = \eta_i - \eta_{jet}$, and the relative azimuthal angle $\Delta\phi_i = \phi_i - \phi_{jet}$ for i -th particle. The input node features $\mathbf{x}_i^{(0)}$ are preprocessed through

$$\mathbf{x}_i^{(0)} = \left(\tan^{-1}(z_i), \frac{\pi}{2} \frac{\Delta\eta_i}{R}, \frac{\pi}{2} \frac{\Delta\phi_i}{R} \right) \text{ with } R = 0.8 \quad (7)$$

The indices of particles are arbitrary, since we will consider permutation invariant models (MPGNN and QCGNN) only.

To balance between the training performance and the enormous training time of quantum machine learning simulation (implemented with classical computers), we randomly select 5000 data³ uniformly distributed in the region $800 \leq p_{Tjet} \leq 1000$ for each channel, with number of particles $2 \leq N \leq 16$, and retaining particles with threshold p_T at least 5% of p_{Tjet} .

B. Classical And Quantum Models

The classical model for benchmarking is based on MPGNN with the aggregation function chosen to be **SUM**. As the datasets are complete graphs, $k = 1$ is set in Eq.(1). Φ is constructed with a fully connected neural network, while leaving γ as the aggregation of Φ only, i.e., $\mathbf{x}_i^{(1)} = \sum_j \Phi(\mathbf{x}_i^{(0)}, \mathbf{x}_j^{(0)})$. Subsequently, the graph feature, denoted as \mathbf{x}^C , will be computed through $\mathbf{x}^C = \sum_i \mathbf{x}_i^{(1)}$ in the last step of MPGNN.

On the other hand, the quantum model is based on QCGNN, consisting of encoding layers and parametrized gates. Additionally, the *data re-uploading* technique [46] is employed before the final measurements (see Fig.1). For simplicity, we use rotation gates, defined as

$$\begin{aligned} R(\alpha, \beta, \gamma) &= R_Z(\gamma) R_Y(\beta) R_Z(\alpha) \\ &= \begin{bmatrix} e^{-i(\alpha+\gamma)/2} \cos(\beta/2) & -e^{-i(\alpha-\gamma)/2} \sin(\beta/2) \\ e^{-i(\alpha-\gamma)/2} \sin(\beta/2) & e^{-i(\alpha+\gamma)/2} \cos(\beta/2) \end{bmatrix}, \end{aligned} \quad (8)$$

² A brief introduction to amplitude encoding provided by PennyLane at https://pennylane.ai/qml/glossary/quantum_embedding/#amplitude-embedding

³ The dataset is generated with fixed random seeds, then separated into 4000 training data and 1000 testing data.

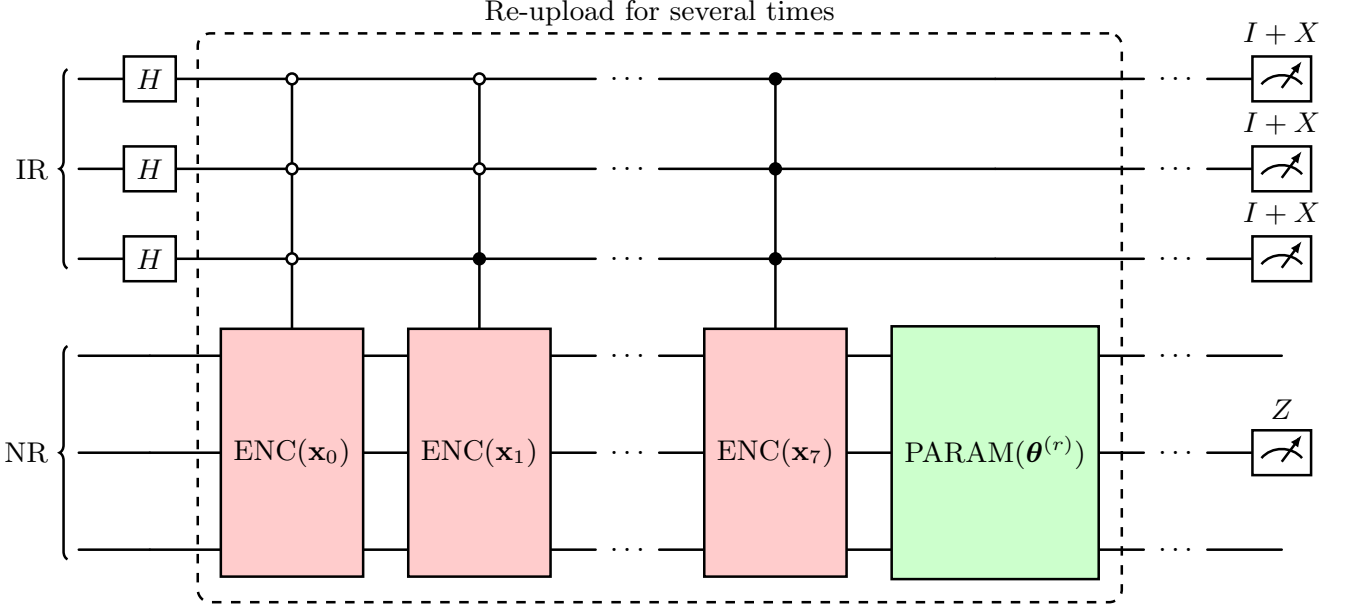


FIG. 1. An example ansatz for learning an 8-node complete graph. At the beginning, IR is initialized with Hadamard gates. The dashed box contains encoding layers and parametrized gates, and can be re-uploaded for several times (the parameters might be different, so we distinguish them with a superscript r). IR will be measured in different combinations of I and X (see Eq.(5, 6)). In this example, the second qubit of NR is measured in Z , corresponding to the second component of the QCGNN output in Eq.(9).

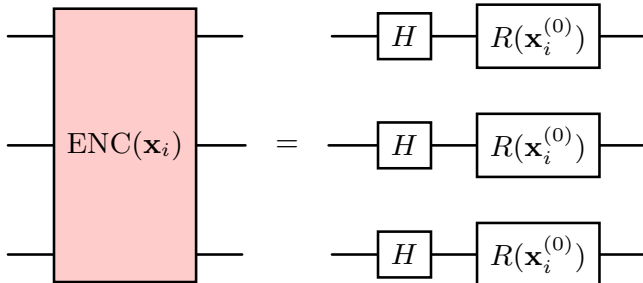


FIG. 2. The ansatz of the encoding block used in QCGNN with $n_Q = 3$, where the rotation gate R is defined in Eq.(8).

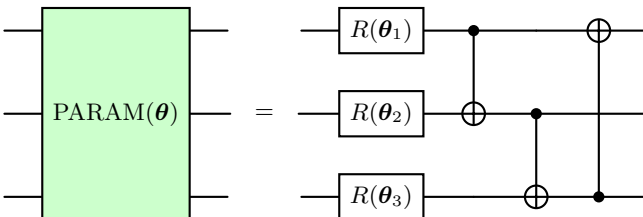


FIG. 3. The ansatz of the strongly entangling layers used in QCGNN with $n_Q = 3$, where the rotation gate R is defined in Eq.(8).

to encode the energy flow information, and the

parametrized gates are constructed with strongly entangling layers [47] using rotation gates. The ansatz for data encoding and the strongly entangling layers are shown in Fig.2 and Fig.3 respectively. The q -th component of the graph feature $\mathbf{x}^Q \in \mathbb{R}^{n_Q}$ is computed by

$$\mathbf{x}_q^Q = \sum_{i \leq j} k(\mathbf{x}_i^{(0)}, \mathbf{x}_j^{(0)}; Z_q^{\text{NR}}), \quad (9)$$

where the observable Z_q^{NR} refers to the Pauli-Z measurement of the q -th qubit in NR, and the sum of two particle correlations k are computed through Eq.(6).

Eventually, both \mathbf{x}^C and \mathbf{x}^Q are followed by a single linear layer to get the final prediction score, and subsequently trained with Adam optimizer by minimizing the binary cross entropy loss. The MPGNN and the QCGNN are implemented using *PyTorch Geometric* [48] and *PennyLane* [49] respectively, with the machine learning framework based on *PyTorch* [50].

IV. RESULTS

A. Training Procedure

Unlike classical computer simulations, we can not use traditional methods such as finite difference to calculate parameter gradients on quantum computers. Instead, we employ the parameter-shift rule (PSR) [35–38] to calculate gradients. However, using PSR on IBMQ requires

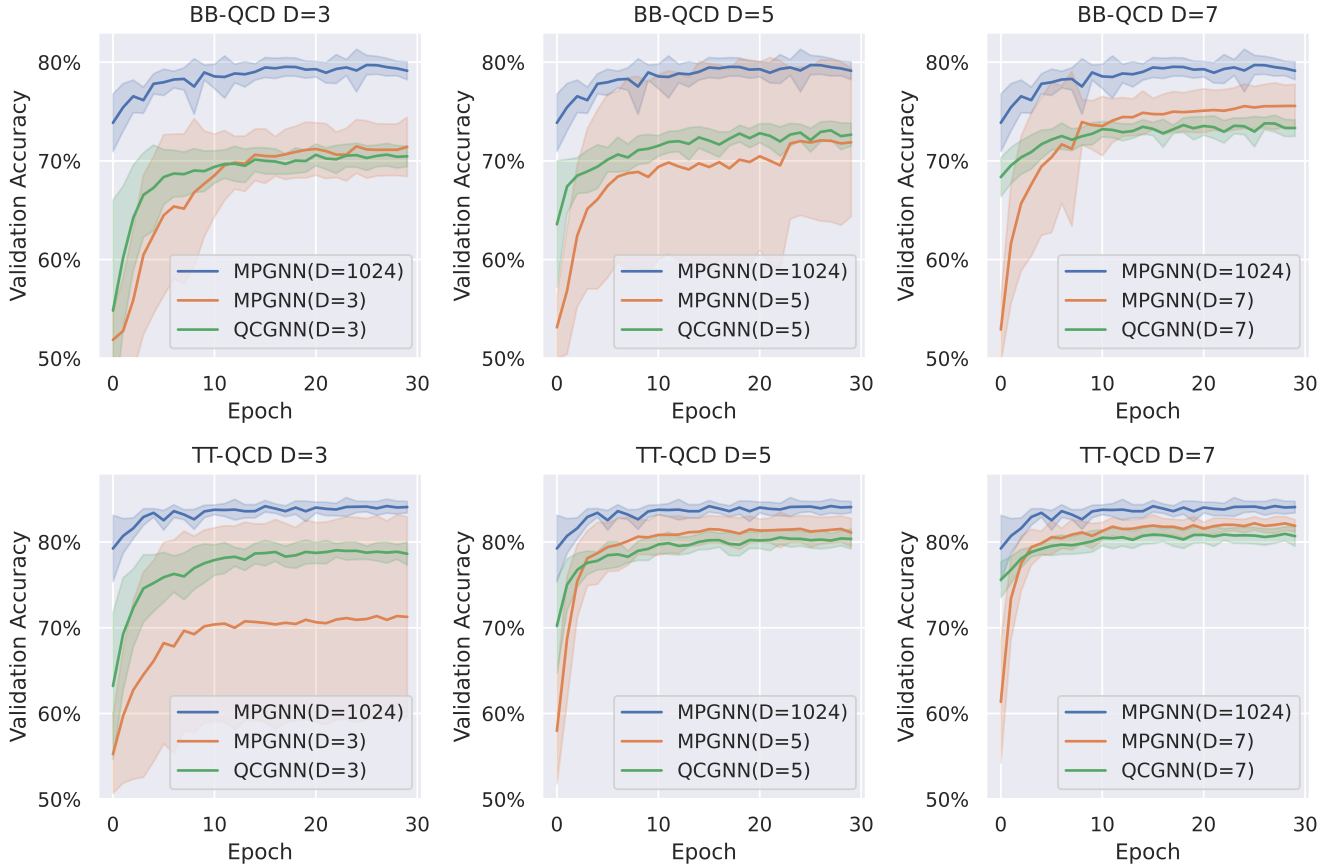


FIG. 4. This figure shows the validation accuracy of MPGNN and QCGNN across 30 epochs. The two rows represent the results for jet discrimination of 2-prong jets ($b\bar{b}$) and 3-prong jets ($t\bar{t}$) against 1-prong jets (QCD) respectively. The colored bandwidth represents the standard deviation of the validation accuracy over 10 random seeds. D denotes the dimension of the hidden neurons of MPGNN or the number of NR qubits in QCGNN.

large request and long queuing time. Additionally, the noise can lead to training failures.

To avoid these issues in the NISQ era, we train QCGNNs on classical computers, using *PennyLane* quantum circuit simulators set to an ideal condition (zero noise). Limited by computational resources, we train the QCGNN with $n_I = 4$ qubits (for a maximum of 16 particles) and $n_Q = \{3, 5, 7\}$ qubits, then data re-upload for $\{3, 5, 7\}$ times. The performance of the pretrained QCGNNs will be tested on IBMQ real devices in section IV B.

For benchmarking, we select the output dimension and the number of hidden neurons in MPGNNs from $\{3, 5, 7\}$, with 2 hidden layers. We also train a relatively powerful MPGNN, with 1024 hidden neurons and 4 hidden layers, to demonstrate the best performance MPGNNs can achieve.

Both QCGNNs and MPGNNs are followed by a single linear layer that transforms the output to one dimension, and subsequently optimized by ADAM optimizer with learning rate 10^{-3} through minimizing the binary cross entropy loss.

Fig.4 shows the comparison of training and validation accuracy for MPGNNs and QCGNNs across 30 epochs. Both classical and quantum models have approximately the same number of parameters and are trained with 10 different random seeds. The prediction power of MPGNN and QCGNN is comparable when the number of parameters is approximately the same. However, the training of QCGNN is more stable, while the MPGNN has larger fluctuations over different random seeds. Besides the training stability, QCGNN also shows a faster training convergence than MPGNN under the same optimization setup, which might lead to a potential quantum advantage when scaling up the quantum model size.

B. Test Pretrained QCGNNs On IBMQ

On IBMQ real devices, only 1-qubit gates and 2-qubit gates are available. The multi-controlled gates used in data encoding must be decomposed, e.g., using methods in [51]. Moreover, in Eq.(2), the quantum state can be arbitrarily initialized through simulators, which are as-

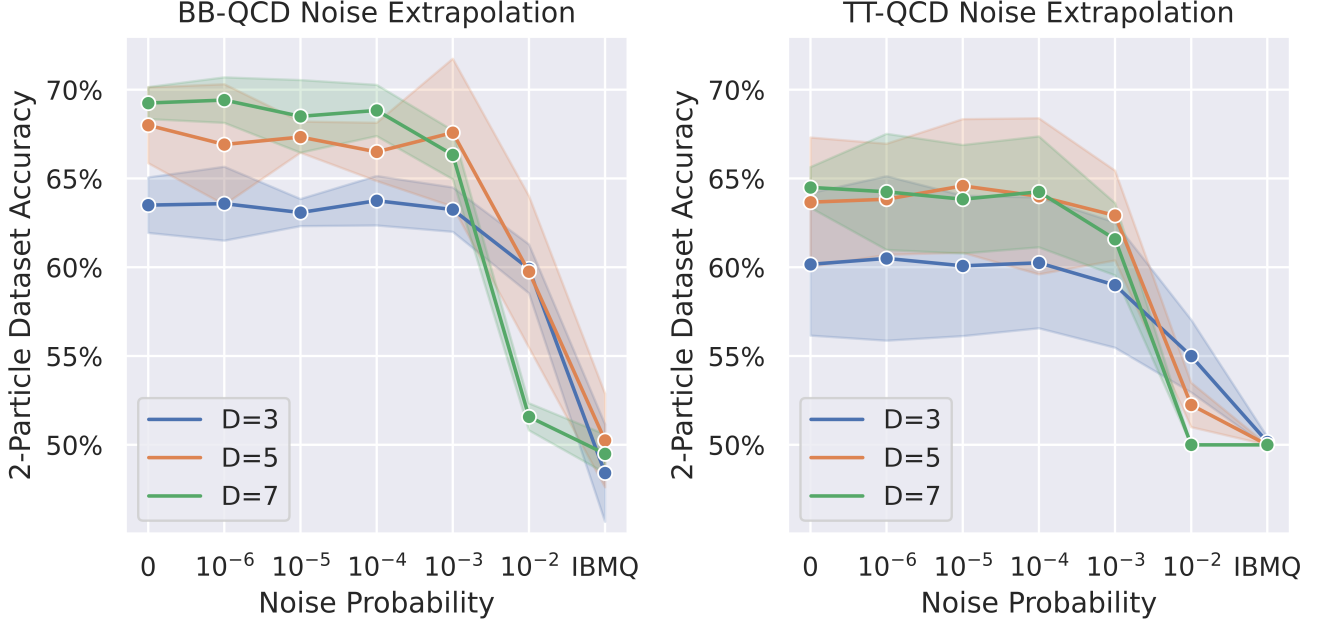


FIG. 5. This figure shows the extrapolation over the probability of noises (depolarizing and amplitude damping) that occur after each quantum operation. Here, D represents the number of NR qubits. An ideal quantum computer corresponds to a 0 noise probability on the x -axis, and "IBMQ" denotes results from running on `ibmq_mumbai`. The y -axis displays the accuracy over 400 jet data up to 2 particles, requiring just 1 IR qubit. The colored bandwidth represents the standard deviation of accuracy across 3 random seeds. Note that the number of data and random seeds differ from the training simulation due to resource limitations on IBMQ.

sumed to be a black box. For the simplest case, we select up to 2 particles for each jet, i.e., only $n_I = 1$ qubit is required, and the initial state can be simply created with a Hadamard gate.

We choose `ibmq_mumbai`⁴ to test the performance of QCGNN on IBMQ real device. However, the quantum computers in the NISQ era are still too noisy to get usable results. To study how the noise affect the performance of QCGNN, we conduct an extrapolation over noise via PennyLane simulators, with results shown in Fig.5. We simulate the quantum noise with *depolarizing error* and *amplitude damping*, which set to occur after each quantum operation at a certain probability. As shown in Fig.5, the probability of noise should be reduced below 10^{-3} to get reliable results⁵.

V. SUMMARY

Owing to the property of permutation invariance, representing jets as graphs has gained prominence in particle physics. However, connecting particles into graphs in a physically reasonable manner remains an open question. Without any specific physical assumptions, we use the most straightforward approach that represents jets using complete graphs with unweighted edges. Motivated by the structure of complete graphs, we propose QCGNN to expedite the training process, particularly for learning with aggregation of two particle correlations through **SUM** or **MEAN**.

To demonstrate the feasibility of QCGNN in jet discrimination, section IV A shows that QCGNN is feasible and comparable to classical models with approximately the same number of parameters. QCGNN also demonstrates a more stable training procedure and faster training convergence over different random seeds. To study how the noise affect the performance, we also conduct an extrapolation over noise via simulators in section IV B.

In summary, QCGNN provides a more efficient way for learning unstructured jets with QML, and is trivial to scale up for the upcoming HL-LHC. Nonetheless, it is still unknown whether QML yields quantum advantages in quantum problems. Moreover, designing a more expressive and suitable method for HEP data encoding

⁴ The calibration of `ibmq_mumbai` at the moment we tested can be obtained from https://drive.google.com/drive/folders/17FiHB1bkYkCIC4Nvx3nyT3HkWpi7WKE?usp=share_link

⁵ The probability of noise here is not equivalent to the gate error or readout error in real devices, but they must be related in certain way.

remains an interesting and ongoing research.

ACKNOWLEDGEMENT

The authors thank Chiao-Hsuan Wang for helpful discussions and suggestions about quantum computation.

The accessibility of IBMQ resource is supported by IBM Quantum Hub at National Taiwan University.

[1] A. Radovic, M. Williams, D. Rousseau, M. Kagan, D. Bonacorsi, A. Himmel, A. Aurisano, K. Terao, and T. Wongjirad, Machine learning at the energy and intensity frontiers of particle physics, *Nature* **560**, 41 (2018).

[2] M. Feickert and B. Nachman, A living review of machine learning for particle physics (2021), [arXiv:2102.02770 \[hep-ph\]](https://arxiv.org/abs/2102.02770).

[3] K.-F. Chen and Y.-T. Chien, Deep learning jet substructure from two-particle correlations, *Phys. Rev. D* **101**, 114025 (2020).

[4] J. S. H. Lee, I. Park, I. J. Watson, and S. Yang, Quark-gluon jet discrimination using convolutional neural networks, *Journal of the Korean Physical Society* **74**, 219 (2019).

[5] P. Baldi, K. Bauer, C. Eng, P. Sadowski, and D. Whiteson, Jet substructure classification in high-energy physics with deep neural networks, *Phys. Rev. D* **93**, 094034 (2016).

[6] P. T. Komiske, E. M. Metodiev, and M. D. Schwartz, Deep learning in color: towards automated quark/gluon jet discrimination, *Journal of High Energy Physics* **2017**, 110 (2017).

[7] J. S. H. Lee, S. M. Lee, Y. Lee, I. Park, I. J. Watson, and S. Yang, Quark gluon jet discrimination with weakly supervised learning, *Journal of the Korean Physical Society* **75**, 652 (2019).

[8] S. Egan, W. Fedorko, A. Lister, J. Pearkes, and C. Gay, Long short-term memory (lstm) networks with jet constituents for boosted top tagging at the lhc (2017), [arXiv:1711.09059 \[hep-ex\]](https://arxiv.org/abs/1711.09059).

[9] J. Pearkes, W. Fedorko, A. Lister, and C. Gay, Jet constituents for deep neural network based top quark tagging (2017), [arXiv:1704.02124 \[hep-ex\]](https://arxiv.org/abs/1704.02124).

[10] H. Qu and L. Gouskos, Jet tagging via particle clouds, *Phys. Rev. D* **101**, 056019 (2020).

[11] S. Gong, Q. Meng, J. Zhang, H. Qu, C. Li, S. Qian, W. Du, Z.-M. Ma, and T.-Y. Liu, An efficient lorentz equivariant graph neural network for jet tagging, *Journal of High Energy Physics* **2022**, 30 (2022).

[12] J. Guo, J. Li, T. Li, and R. Zhang, Boosted higgs boson jet reconstruction via a graph neural network, *Phys. Rev. D* **103**, 116025 (2021).

[13] I. Henrion, J. Brehmer, J. Bruna, K. Cho, K. Cranmer, G. Louppe, and G. Rochette, Neural message passing for jet physics (2017).

[14] J. Shlomi, P. Battaglia, and J.-R. Vlimant, Graph neural networks in particle physics, *Machine Learning: Science and Technology* **2**, 021001 (2020).

[15] S. Thais, P. Calafiura, G. Chachamis, G. DeZoort, J. Duarte, S. Ganguly, M. Kagan, D. Murnane, M. S. Neubauer, and K. Terao, Graph neural networks in particle physics: Implementations, innovations, and challenges (2022), [arXiv:2203.12852 \[hep-ex\]](https://arxiv.org/abs/2203.12852).

[16] J. Biamonte, P. Wittek, N. Pancotti, P. Rebentrost, N. Wiebe, and S. Lloyd, Quantum machine learning, *Nature* **549**, 195 (2017).

[17] A. Zeguendry, Z. Jarir, and M. Quafafou, Quantum machine learning: A review and case studies, *Entropy* **25**, 10.3390/e25020287 (2023).

[18] D. P. García, J. Cruz-Benito, and F. J. García-Péñalvo, Systematic literature review: Quantum machine learning and its applications (2022), [arXiv:2201.04093 \[quant-ph\]](https://arxiv.org/abs/2201.04093).

[19] K. A. Tychola, T. Kalampokas, and G. A. Papakostas, Quantum machine learning mdash;an overview, *Electronics* **12**, 10.3390/electronics12112379 (2023).

[20] M. Schuld and F. Petruccione, *Machine Learning with Quantum Computers* (2021).

[21] W. Guan, G. Perdue, A. Pesah, M. Schuld, K. Terashi, S. Vallecorsa, and J.-R. Vlimant, Quantum machine learning in high energy physics, *Machine Learning: Science and Technology* **2**, 011003 (2021).

[22] Tüysüz, Cenk, Carminati, Federico, Demirköz, Bilge, Dobos, Daniel, Fracas, Fabio, Novotny, Kristiane, Potamianos, Karolos, Vallecorsa, Sofia, and Vlimant, Jean-Roch, Particle track reconstruction with quantum algorithms, *EPJ Web Conf.* **245**, 09013 (2020).

[23] K. Terashi, M. Kaneda, T. Kishimoto, M. Saito, R. Sawada, and J. Tanaka, Event classification with quantum machine learning in high-energy physics, *Computing and Software for Big Science* **5**, 2 (2021).

[24] S. L. Wu, J. Chan, W. Guan, S. Sun, A. Wang, C. Zhou, M. Livny, F. Carminati, A. D. Meglio, A. C. Y. Li, J. Lykken, P. Spentzouris, S. Y.-C. Chen, S. Yoo, and T.-C. Wei, Application of quantum machine learning using the quantum variational classifier method to high energy physics analysis at the lhc on ibm quantum computer simulator and hardware with 10 qubits, *Journal of Physics G: Nuclear and Particle Physics* **48**, 125003 (2021).

[25] A. Ganelle, P. Koppenburg, D. Lucchesi, D. Nicotra, E. Rodrigues, L. Sestini, J. de Vries, and D. Zuliani, Quantum machine learning for b-jet charge identification, *Journal of High Energy Physics* **2022**, 14 (2022).

[26] M. Cerezo, A. Arrasmith, R. Babbush, S. C. Benjamin, S. Endo, K. Fujii, J. R. McClean, K. Mitarai, X. Yuan, L. Cincio, and P. J. Coles, Variational quantum algorithms, *Nature Reviews Physics* **3**, 625 (2021).

[27] A. Peruzzo, J. McClean, P. Shadbolt, M.-H. Yung, X.-Q. Zhou, P. J. Love, A. Aspuru-Guzik, and J. L. O'Brien, A variational eigenvalue solver on a photonic quantum processor, *Nature Communications* **5**, 4213 (2014).

[28] J. R. McClean, J. Romero, R. Babbush, and A. Aspuru-Guzik, The theory of variational hybrid quantum-classical algorithms, *New Journal of Physics* **18**, 023023

(2016).

[29] E. W. Weisstein, "complete graph." from [mathworld—a wolfram web resource](#), last visited on 2/11/2023.

[30] W. Fan, Y. Ma, Q. Li, Y. He, E. Zhao, J. Tang, and D. Yin, Graph neural networks for social recommendation (2019), [arXiv:1902.07243 \[cs.IR\]](#).

[31] X.-M. Zhang, L. Liang, L. Liu, and M.-J. Tang, Graph neural networks and their current applications in bioinformatics, *Frontiers in Genetics* **12**, 10.3389/fgene.2021.690049 (2021).

[32] P. Reiser, M. Neubert, A. Eberhard, L. Torresi, C. Zhou, C. Shao, H. Metni, C. van Hoesel, H. Schopmans, T. Sommer, and P. Friederich, Graph neural networks for materials science and chemistry, *Communications Materials* **3**, 93 (2022).

[33] J. Gilmer, S. S. Schoenholz, P. F. Riley, O. Vinyals, and G. E. Dahl, Neural message passing for quantum chemistry (2017), [arXiv:1704.01212 \[cs.LG\]](#).

[34] J. Preskill, Quantum Computing in the NISQ era and beyond, *Quantum* **2**, 79 (2018).

[35] K. Mitarai, M. Negoro, M. Kitagawa, and K. Fujii, Quantum circuit learning, *Phys. Rev. A* **98**, 032309 (2018).

[36] M. Schuld, V. Bergholm, C. Gogolin, J. Izaac, and N. Killoran, Evaluating analytic gradients on quantum hardware, *Phys. Rev. A* **99**, 032331 (2019).

[37] D. Wierichs, J. Izaac, C. Wang, and C. Y.-Y. Lin, General parameter-shift rules for quantum gradients, *Quantum* **6**, 677 (2022).

[38] G. E. Crooks, Gradients of parameterized quantum gates using the parameter-shift rule and gate decomposition (2019), [arXiv:1905.13311 \[quant-ph\]](#).

[39] J. Alwall, R. Frederix, S. Frixione, V. Hirschi, F. Maltoni, O. Mattelaer, H. S. Shao, T. Stelzer, P. Torrielli, and M. Zaro, The automated computation of tree-level and next-to-leading order differential cross sections, and their matching to parton shower simulations, *JHEP* **07**, 079, [arXiv:1405.0301 \[hep-ph\]](#).

[40] C. Bierlich, S. Chakraborty, N. Desai, L. Gellersen, I. Hedenius, P. Ilten, L. Lönnblad, S. Mrenna, S. Prestel, C. T. Preuss, T. Sjöstrand, P. Skands, M. Utheim, and R. Verheyen, A comprehensive guide to the physics and usage of pythia 8.3 (2022), [arXiv:2203.11601 \[hep-ph\]](#).

[41] S. Ovyn, X. Rouby, and V. Lemaitre, Delphes, a framework for fast simulation of a generic collider experiment (2010), [arXiv:0903.2225 \[hep-ph\]](#).

[42] J. de Favereau, C. Delaere, P. Demin, A. Giannanco, V. Lemaître, A. Mertens, and M. Selvaggi (DELPHES 3), DELPHES 3, A modular framework for fast simulation of a generic collider experiment, *JHEP* **02**, 057, [arXiv:1307.6346 \[hep-ex\]](#).

[43] M. Cacciari, G. P. Salam, and G. Soyez, The anti-kt jet clustering algorithm, *Journal of High Energy Physics* **2008**, 063 (2008).

[44] M. Cacciari, G. P. Salam, and G. Soyez, Fastjet user manual, *The European Physical Journal C* **72**, 1896 (2012).

[45] D. Pappadopulo, A. Thamm, R. Torre, and A. Wulzer, Heavy Vector Triplets: Bridging Theory and Data, *JHEP* **09**, 060, [arXiv:1402.4431 \[hep-ph\]](#).

[46] A. Pérez-Salinas, A. Cervera-Lierta, E. Gil-Fuster, and J. I. Latorre, Data re-uploading for a universal quantum classifier, *Quantum* **4**, 226 (2020).

[47] M. Schuld, A. Bocharov, K. M. Svore, and N. Wiebe, Circuit-centric quantum classifiers, *Phys. Rev. A* **101**, 032308 (2020).

[48] M. Fey and J. E. Lenssen, Fast graph representation learning with PyTorch Geometric, in *ICLR Workshop on Representation Learning on Graphs and Manifolds* (2019).

[49] V. Bergholm, J. Izaac, M. Schuld, C. Gogolin, S. Ahmed, V. Ajith, M. S. Alam, G. Alonso-Linaje, B. Akash-Narayanan, A. Asadi, J. M. Arrazola, U. Azad, S. Banning, C. Blank, T. R. Bromley, B. A. Cordier, J. Ceroni, A. Delgado, O. D. Matteo, A. Dusko, T. Garg, D. Gual, A. Hayes, R. Hill, A. Ijaz, T. Isacsson, D. Ittah, S. Jhangiri, P. Jain, E. Jiang, A. Khandelwal, K. Kottmann, R. A. Lang, C. Lee, T. Loke, A. Lowe, K. McKiernan, J. J. Meyer, J. A. Montañez-Barrera, R. Moyard, Z. Niu, L. J. O'Riordan, S. Oud, A. Panigrahi, C.-Y. Park, D. Polatajko, N. Quesada, C. Roberts, N. Sá, I. Schoch, B. Shi, S. Shu, S. Sim, A. Singh, I. Strandberg, J. Soni, A. Száva, S. Thabet, R. A. Vargas-Hernández, T. Vincent, N. Vitucci, M. Weber, D. Wierichs, R. Wiersema, M. Willmann, V. Wong, S. Zhang, and N. Killoran, PennyLane: Automatic differentiation of hybrid quantum-classical computations (2022), [arXiv:1811.04968 \[quant-ph\]](#).

[50] P. Team, Pytorch.

[51] M. A. Nielsen and I. L. Chuang, Controlled operations, in *Quantum Computation and Quantum Information* (Cambridge University Press, 2007) Chap. 4.3 Fig(4.10).